Quasi-Action Variable for Chaos in Chemical Dynamics†

Kazuo TAKATSUKA
Graduate School of Human Informatics, Nagoya University, Nagoya 464-01
(Received May 10, 1993)

Is proposed quasi-action variable as a means to analyze the onset of classical chaos in molecular vibrational systems. The basic idea rests on a symplectic area generated by a classical trajectory in phase space, from which the geometrical information of a torus and its breakdown in extracted. The Fourier spectrum of the time derivative of this symplectic area centers on the following definition and findings: (1) in an integrable system, the action variables can be simply calculated in terms of the above Fourier amplitudes, (2) the quasi-action variable is also defined in a similar way and is a good approximation to the corresponding action variable, but (3) the construction of the quasi-action variable does not depend on the integrability and hence it it defined as well even for a chaotic system, and (4) the characteristics of chaos can be analyzed in the continuous spectrum of the quasi-action variable. Some numerical examples of the quasi-action variable are presented for a system of what we call phase-space large amplitude motion. As a byproduct, a simple method has been devised to calculate very accurate frequencies and amplitudes from the so-called Fast-Fourier-Transform (FFT) spectra without resorting to the so-called window technique.

Onset of chaos[1] is an important issue in chemical dynamics. Strong chaos is generally believed to dominate energy flow occurring among vibrational modes in the dynamical processes of reaction and structural deformation, since chaotic energy transfer is generally believed to introduce the statistical nature into pure (or deterministic) dynamics. The energy flow among the large number of coupled nonlinear oscillators can happen to bring a massive energy onto small number of localized modes. This is also likely to be the case for large molecular systems including macro-molecules, clusters and even liquid phase, because large systems generally tend to have shallow and anharmonic potential surfaces due to weak inter-molecular interactions. On the other hand, in a weak chaos in the onset energy range, a new class of large amplitude motion, the so-called phase-space large amplitude motion,[2] is predicted to be observed. This particular vibrational mode is expected to generate a quite strange and unpredictable time series.

Classical chaos in a Hamiltonian system is defined in the notion of breakdown of an invariant torus (a doughnut structure in phase space), the size of which is measured in terms of the action variables. Therefore, the action variable is one of the most fundamental quantities in classical dynamics.[3] In addition, it is invariant under the canonical transformation and adiabatic changes. The adiabatic invariance generally implies the slowest mode among the available motions. In classical mechanics, it is simply a constant of motion. It is also well-known that the EBK (Einstein–Brillouin–Keller) conditions[4] require to quantize the action variables for the semiclassical evaluation of quantum energies. Hence the importance of the action variable cannot be overemphasized. On the other hand, however, if the torus is broken, in other words, if chaos takes place, the action variables are not defined any longer in a straightforward manner.[1]

For a system with relatively small number of degrees of freedom, various methods to calculate the action variables have already been devised, which are listed extensively in the papers by Martens and Ezra.[5,6] They themselves also have proposed a method based on the idea of Percival:[7] The Fourier amplitudes and frequencies of the position in configuration space of each molecular nucleus $q_i(t)$ are determined numerically, since they are known to be multiply-periodic.[3] Then all these Fourier data are inserted directly into the definition of the action variables. Although this method (more precisely, not only this method) potentially should have some practical difficulty that would be apparent with increasing degrees of freedom, the theory seems excellent. Nonetheless, chaos requires to shed another light on the phase-space geometry of dynamics, simply because the action variable is not defined there.

In the present paper, we propose a quantity which is closely analogous to the action variable, and yet can be determined every stage of dynamics, either regular or chaotic. Thus this is a kind of natural generalization of the action variable so as to cover chaotic dynamics. For this purpose, we first consider a geometrical quantity, denoted by $B'(t)$, which is generated by a classical trajectory in phase space. $B'(t)$ is of symplectic and canonical invariance.[1] In an integrable case, $B'(t)$ provides a Fourier line-spectrum and the action variables are calculated directly from these Fourier amplitudes. Furthermore, making use of the same Fourier data, one can define a quantity that is akin to the action variable. We call this quantity the quasi-action variable. However, the quasi-action variable is sharply different from the action variable in that the former can be defined even in chaos.

The quasi-action variable is a continuous function of the frequency if a system is not integrable. Naturally, the quasi-action variable in chaos is not a constant of

†To the memory of the late Professor Hiroshi Kato.

motion and hence becomes smaller as time passes. The decay of the correlation function based on $B'(t)$ can be used to detect the onset of chaos with extremely high sensitivity. This is because the existence of the action variable is directly monitored. Also, it represents the nature of chaos. Therefore, one can investigate various mechanisms of onset of chaos by examining the patterns of the quasi-action variable. Some of such numerical examples will be presented in the present paper.

As a byproduct of the present study, we have devised a new method to extract extremely accurate frequencies and amplitudes[8] from Fast-Fourier-Transform (FFT)[9] spectra. FFT is well-known as an ultra-fast approximation to the Fourier transformation. However, it is also well-known that it gives neither accurate frequencies nor correct amplitudes, simply because it is a discrete transformation and because the so-called Gibbs phenomenon creates artificial tails due to the unavoidable practice of using a truncated (finite length of) data set. A standard way of improving the situation is repeated applications of the so-called window technique.[5] However, the window method is very tedious in general. We will show that one can obtain the accurate frequencies and amplitudes of any discrete spectrum without use of such windows.

The organization of the present paper is as follows. Our study begins with defining $B'(t)$ is Sect. I. In Sect. II, it is shown first how the action variables can be determined from the Fourier spectrum of $B'(t)$. Section III covers a practical method to calculate frequencies and amplitudes from FFT spectra. In Sect. IV, we define the quasi-action variable for chaos on the basis of the geometry discussed in Sects. I and II. In Sect. V, the quasi-action variable is numerically presented with an application to a very weak chaos in an onset region.

I. Geometrical Background

A. Geometrical Objects Induced by a Trajectory. Suppose that we have a classical trajectory in a $2N$ dimensional phase space as depicted in Fig. 1. Let $\vec{Z}(t)=(\vec{Z}_i(t))=(q_i(t),p_i(t))$ $(i=1,2,\cdots,N)$ be a point on the trajectory at time t, where $q_i(t)$ and $p_i(t)$ indicate the i-th Cartesian coordinates of position and its conjugate momentum, respectively. $\vec{O}=(0,0)$ is the origin of the coordinate system. We define the following oriented areas (see Figs. 1 and 2):

(i) The sector (fan) made by $OZ(t)Z(0)$,

$$Fan(t)=\frac{1}{2}\sum_{n=0}^{M-1}\sum_{i=1}^{N}\vec{Z}_i(t_n)\wedge\vec{Z}_i(t_n+\Delta t)\quad(\Delta t\to 0),\quad(1)$$

where $t_0=0$, $t_n=n\Delta t$, and $M=t/\Delta t$. The limit $\Delta t\to 0$ is to be taken after all the calculations up to Eq. 4 are over. The 2-form in this equation is defined by[3]

$$Z_i(t_m)\wedge Z_i(t_n)=p_i(t_m)q_i(t_n)-q_i(t_m)p_i(t_n),\quad(2)$$

the geometrical meaning of which is a symplectic area

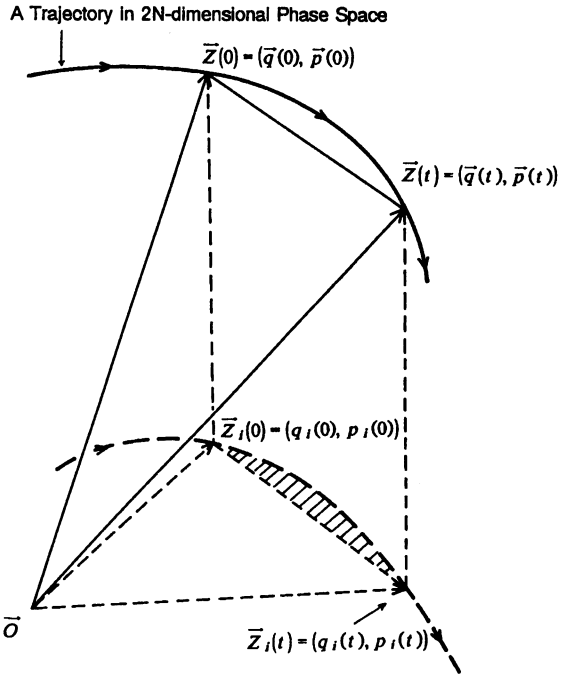

Fig. 1. A classical trajectory running in $2N$-dimensional Cartesian phase space. It is projected onto the i-th canonical sub-plane. The shaded areas in all the sub-planes are summed up to build a symplectic area $B(t)$.

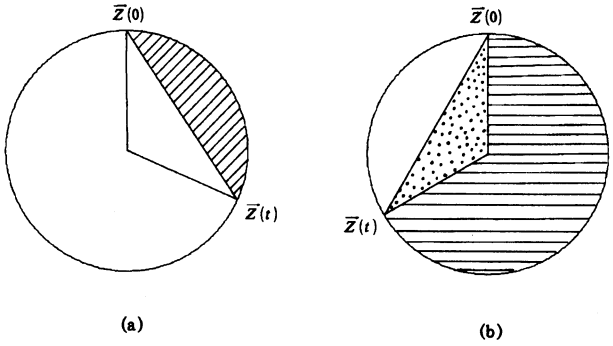

Fig. 2. The construction of $B(t)$ in the Cartesian phase space for a harmonic oscillator. The (sum of the) shaded areas corresponds to $B(t)$. In (b), the triangle has a negative value and $B(t)$ is the total area swept by the line $Z(0)Z(t)$.

made by the two $2N$-dimensional vectors $\vec{Z}(t_m)$ and $\vec{Z}(t_n)$ projected onto the i-th phase sub-plane.

(ii) A triangle area made by $OZ(t)Z(0)$, which is defined by

$$A(t)=\frac{1}{2}\sum_{i=1}^{N}\vec{Z}_i(0)\wedge\vec{Z}_i(t).\quad(3)$$

Obviously, this quantity can become negative.

(iii) The chord area defined by

$$B(t)=Fan(t)-A(t)=\sum_i B_i(t).\quad(4)$$

The shaded area in Fig. 1 is an example of B_i. Note

that the sum of all the above two-forms, as performed in Eqs. 1, 3, and 4, is symplectically and canonically invariant. Therefore, the summed quantity does not depend on the choice of canonical coordinates,[3] although each term as in Eq. 2 strongly does. It is almost obvious from the above construction that the symplectic area swept by the straight line $OZ(t)$, that is $B(t)$, should be directly related to the action integral and hence to the action variables. Thus the central quantities to be investigated in what follows are $B(t)$ and its time derivative.

B. An Example from a One-Dimensional Harmonic Oscillator. In order to materialize the above definitions in an intuitive picture, let us consider a one-dimensional harmonic oscillator. The action variable is defined as[3]

$$I = \frac{1}{2\pi}\oint p\mathrm{d}q \tag{5}$$

and the frequency ω is given by[3]

$$\omega = \frac{\partial H}{\partial I}. \tag{6}$$

(A harmonic oscillator happens to have $H=I\omega$) Then it is straightforward to obtain

$$Fan(t) = I\omega t, \tag{7}$$

$$A(t) = I\sin(\omega t), \tag{8}$$

and

$$B(t) = I(\omega t - \sin(\omega t)). \tag{9}$$

These areas are schematically drawn in Fig. 2. $Fan(t)$ increases linearly with t. $A(t)$ is a periodically oscillating function and becomes negative after $t=T/2$ and comes back to zero at $t=T$, where T is the period ($\omega T=2\pi$). Thus $B(t)$ is a linearly increasing function with the oscillatory component(s) superposed. Since $B(t)$ is the oriented area swept by the straight line $Z(0)Z(t)$, we simply have $B(T)=2\pi I$.

It is also trivial to see $Fan(T)=2\pi I$. However, it is hard to pick up information from the time derivative of $Fan(t)$, since it is merely a constant. On the other hand, the time derivative of $B(t)$ has a form

$$B'(t) = I\omega(1-\cos(\omega t)), \tag{10}$$

where the compact information on both frequency and action variable is available, which can be extracted by means of the Fourier transformation.

C. Direct Calculation of $B'(t)$. As shown above, it has turned out that the spectral data of $B'(t)$ are all we need. Here, we present a simpler expression of $B'(t)$ for practical computation. First we note

$$\begin{aligned} B(t+\Delta t) - B(t) &= \frac{1}{2}\sum_{i=1}^{N}\left[\vec{Z}_i(t)\wedge\vec{Z}_i(t+\Delta t)\right. \\ &\left. -\vec{Z}_i(0)\wedge\vec{Z}_i(t+\Delta t) + \vec{Z}_i(0)\wedge\vec{Z}_i(t)\right] \\ &= \frac{1}{2}\sum_{i=1}^{N}\left[\left\{\vec{Z}_i(t)-\vec{Z}_i(0)\right\}\wedge\left\{\vec{Z}_i(t+\Delta t)-\vec{Z}_i(t)\right\}\right]. \end{aligned} \tag{11}$$

On the other hand, the canonical equations of motion

$$\frac{\mathrm{d}q_i}{\mathrm{d}t} = \frac{\partial H}{\partial p_i} \quad\text{and}\quad \frac{\mathrm{d}p_i}{\mathrm{d}t} = -\frac{\partial H}{\partial q_i} \tag{12}$$

are rewritten collectively in a finite difference form as

$$\frac{\vec{Z}_i(t+\Delta t)-\vec{Z}_i(t)}{\Delta t} = \vec{f}_i(t) \tag{13}$$

with the obvious notation of $\vec{f}_i$. Combining these equations, we have

$$\frac{B(t+\Delta t)-B(t)}{\Delta t} = \frac{1}{2}\sum_{i=1}^{N}\left[\vec{Z}_i(t)-\vec{Z}_i(0)\right]\wedge\vec{f}_i(t). \tag{14}$$

Here the limit $\Delta t\to 0$ should be taken. Thus it turns out that only the quantities that are required to run a classical trajectory suffice to evaluate $B'(t)$. In addition, $B'(t)$ of Eq. 14 can be generated at any instance with an arbitrary time-interval. $B'(t)\Delta t$ in Eq. 14 clearly indicates its geometrical meaning again, that is an oriented area the line $Z(0)Z(t)$ sweeps in phase space during Δt.

II. Integrable Cases and Action Variables

Although our main concern is in chaotic dynamics, we first show in this section that $B'(t)$ is indeed related to the action variable.

A. Expansions of $B(t)$ and $B'(t)$. We first consider a one-dimensional anharmonic oscillator in the action-angle coordinates in Fig. 3, which is transformed from the Cartesian geometry described above. The straight line in Fig. 3 indicates a trajectory, the action of which is a constant. The curved line convex downward corresponds to the line connecting $Z(0)$ and $Z(t)$, which is straight in the Cartesian view as in Fig. 2. As $Z(t)$ in Fig. 3a approach $\theta=\pi$ (θ denotes the angle coordinate), the curved line comes down more and more deeply, and concomitantly the shaded area for $B(t)$ increases up to πI until $\theta=\pi$. After passing $\theta=\pi$, $B(t)$ changes its topology as in Fig. 3b and at $\theta=2\pi n$ ($t=nT$, with n integer) we have $B(nT)=2\pi nI$.

We next treat a multi-dimensional case. First of all, because of the canonically invariant construction of $B(t)$, Eq. 4 is reexpressed as the direct sum of the contributions from the individual action-angle plane,

$$\begin{aligned} B(t) &= \sum_{i=1}^{N} B_i(t) = \sum_{k=1}^{N} B_k(t) \\ \text{and}\quad B'(t) &= \sum_{i=1}^{N} B_i'(t) = \sum_{k=1}^{N} B_k'(t). \end{aligned} \tag{15}$$

[In what follows, the suffix i is used for the Cartesian coordinates as in Eq. 4, and k for the action-angle coordinates.] This is straightforward from the theorem of the absolute integral invariance due to Poincaré and Cartan.[3] Then the above geometrical situation for one-dimension is essentially similar to that in each k-th coordinate (again in Fig. 3), with an important exception that the multiply-periodicity of $B_k(t)$ manifests itself.

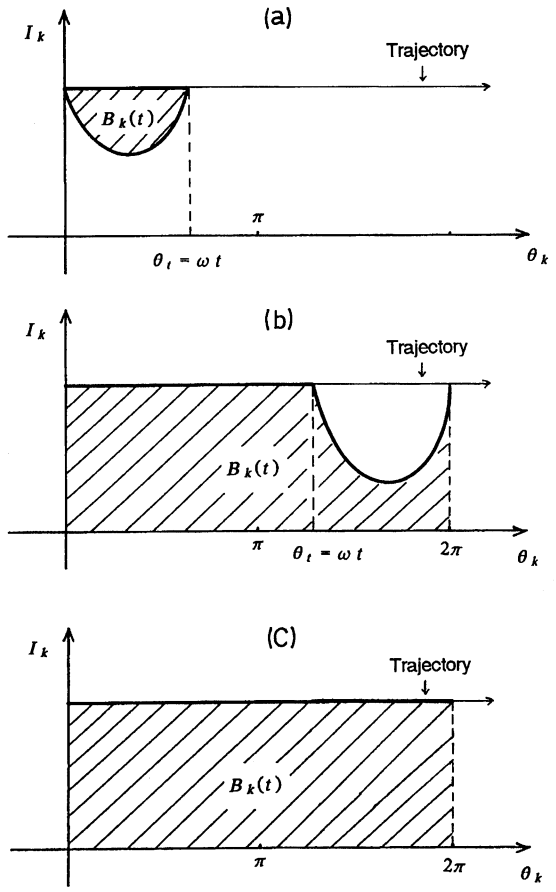

Fig. 3. The construction of $B(t)$ in the action-angle phase space. The shaded areas represents $B(t)$.

To be more precise, the curve convex downward representing $Z(0)Z(t)$ depends on where the current point $Z(t)$ is located. Thus the area $B_k(t)$ is a function not only of ω_k but also of $\omega_h (h \neq k)$, where ω_k, for example, is the frequency in the k-th action-angle coordinates.

On the other hand, the $B_k(t)$ should have a quasi-recurrent property in the sense that

$$B_k(nT_k) = 2\pi n I_k, \tag{16}$$

where T_k $(=2\pi/\omega_k)$ is the period, and n is an integer. This requirement arises geometrically as follows: At each time when θ_k passes through the value 2π (mod. 2π), the topology of Fig. 3b has to come back to that of Fig. 3a through the full shape given in Fig. 3c. But, this shape is realized only at $\theta_k = 2\pi$ (mod. 2π), because if this were not the case [i.e. if the topology of Fig. 3c were formed at an angle other than $\theta_k = 2\pi$ (mod. 2π)], the convex line representing $Z(0)Z(t)$ had to coincide with the classical trajectory itself. This cannot happen in general as long as a trajectory forms a curved line in phase space. In other words, only through the recurrent configuration of Fig. 3c at $\theta_k = 0$ (mod. 2π), the topology of the shaded area can be connected smoothly. It is obvious then that the configuration in Fig. 3c immediately leads to Eq. 16.

Taking account of the multiply-periodicity and quasi-recurrence, one can expand $B_k(t)$ as

$$B_k(t) = a^k t + \sum_{m \geq 0} \left[b_m^k \sin(m\omega_k t) + c_m^k \cos(m\omega_k t) \right] + \sum_m \sin(m\omega_k t) G_m^k(t). \tag{17}$$

The first term in the right hand side indicates the linear increase of $B_k(t)$ and the second term in the sum form represents its own periodicity. $G_m^k(t)$ has been introduced so as to take account of the multiply-periodicity. Hence, $G_m^k(t)$ is a function of all the frequencies other than ω_k. Although $G_m^k(t)$ can generate complicated combination bands associated with the frequency $m\omega_k$, it is not necessary here to expand $G_m^k(t)$ in the Fourier series. The quasi-recurrence property allows $G_m^k(t)$ to appear only in the part of the sine-function. With no loss of generality, it is always assumed that

$$G_m^k(0) = 0. \tag{18}$$

If this is not the case, the non-zero value $G_m^k(0)$ can be subtracted from $G_m^k(t)$ to make it zero at $t=0$, and then the subtracted value is recovered as a part of b_m^k.

B. Action Variables from $B'(t)$. B-1. Non-Resonant Case. The geometry of Fig. 3 imposes the following three conditions on $B_k(t)$ and $B_k'(t)$, from which the action variable can be calculated.

(1) $B_k(0)=0$, which requires

$$\sum_{m \geq 0} c_m^k = 0. \tag{19}$$

(2) $B_k(T_k)=2\pi I_k$, which means

$$a^k T_k + \sum_{m \geq 0} c_m^k = 2\pi I_k. \tag{20}$$

(3) $B_k'(0)=0$. From Eq. 17, we have

$$B_k'(t) = a^k + \sum_{m \geq 0} m\omega_k \left[b_m^k \cos(m\omega_k t) - c_m^k \sin(m\omega_k t) \right] + \sum_m \left[m\omega_k \cos(m\omega_k t) G_m^k(t) + \sin(m\omega_k t) G_m^{k'}(t) \right]. \tag{21}$$

With the help of Eq. 18, this condition turns out to be

$$a^k + \omega_k \sum_{m \geq 0} m b_m^k = 0 \tag{22}$$

This last condition is geometrically obvious if we look at Fig. 3a, where the convex line is infinitely close to the straight line representing the classical trajectory in the limit of $t=0$ and $\Delta t=0$. Equation 14 proves this statement analytically. It turns out that these conditions do not include any effect from $G_m^k(t)$.

From Eqs. 19 and 20, it follows that

$$I_k = \frac{a^k T_k}{2\pi} = \frac{a^k}{\omega_k}. \tag{23}$$

Therefore, obtaining I_k is equivalent to calculating a^k, provided that ω_k is known. However, except for one-

dimensional cases, it is impossible to resolve the zero-frequency amplitude of $B'(t)$ to each component a^k independently, since only their sum $\sum a^k$ is available. Alternatively, using Eq. 22, one can represent

$$I_k = -\sum_{m=1} m b_m^k. \tag{24}$$

Note that all the required components b_m^k in this expression can be identified in the fundamental frequency and its harmonics of the spectrum for a single quantity $B'(t)$.

B-2. Resonant Cases. The procedure described above can be extended to a system of resonance. Martens and Ezra[6] have already presented a thorough analysis on resonance, to which we can add nothing new. Here we only show that our theory can be extended to the resonant cases in a straightforward manner.

(i) Primary Resonance. Suppose that we have a primary resonance between the k-th and h-th coordinates in such a way that

$$n_h\omega_k = n_k\omega_h, \tag{25}$$

where the coefficients in Eq. 25 are the positive integers. (If a system under study is two dimensional, the resultant orbit is completely periodic. The extension to a case where more than two coordinates resonate is straightforward.) Note that the commensurable relation here is assumed in the full (or perturbed) Hamiltonian. In this case, the k–h subspace has a new fundamental frequency given by

$$\omega_{kh}^R = \frac{\omega_k}{n_k} = \frac{\omega_h}{n_h}, \tag{26}$$

and all the other frequencies related to this subspace can be regarded as the harmonics of ω_{kh}^R. Once Eq. 25 holds, the functions $B(t)$ and $B'(t)$ in these coordinates must be treated collectively as

$$\begin{aligned} B_{kh}(t) = a_R^{kh}t + \sum_{m\geq 0}\Big[b_{R,m}^{kh}\sin(m\omega_{kh}^R t) \\ + c_{R,m}^{kh}\cos(m\omega_{kh}^R t)\Big] \\ + \sum_m \sin(m\omega_{kh}^R t)G_{R,m}^{kh}(t). \end{aligned} \tag{27}$$

Here again $G_{R,m}^{kh}(t)$ represents the multiply-periodicity and is the function of the other frequencies. It is supposed to hold that

$$G_{R,m}^{kh}(0) = 0, \tag{28}$$

The derivative of $B_{kh}(t)$ then follows as

$$\begin{aligned} B'_{kh}(t) = a_R^{kh} + \sum_{m\geq 0} m\omega_{kh}^R\Big[b_{R,m}^{kh}\cos(m\omega_{kh}^R t) \\ - c_{R,m}^{kh}\sin(m\omega_{kh}^R t)\Big] \\ + \sum_m \Big[m\omega_{kh}^R\cos(m\omega_{kh}^R t)G_{R,m}^{kh}(t) \\ + \sin(m\omega_{kh}^R t)G_{R,m}^{kh\prime}(t)\Big]. \end{aligned} \tag{29}$$

It is clear from Eqs. 27 and 29 that the Fourier transformation does not resolve the amplitudes belonging to ω_k and ω_h as the independent quantities.

As before, the conditions are imposed on $B_{kh}(t)$ and its derivative.

(1) $B_{kh}(0)=0$, which requires

$$\sum_{m\geq 0} c_{R,m}^{kh} = 0. \tag{30}$$

(2) $B'_{kh}(0)=0$, which gives rise to

$$a_R^{kh} + \omega_{kh}^R \sum_{m\geq 0} m b_{R,m}^{kh} = 0. \tag{31}$$

(3) The period in the k-h coordinates is given by

$$T_{kh} = n_k T_k = n_h T_h, \quad T_k = \frac{2\pi}{\omega_k} \text{ and } T_h = \frac{2\pi}{\omega_h}. \tag{32}$$

And $B_{kh}(T_{kh})=2\pi I_{kh}$, which means

$$a_R^{kh}T_{kh} + \sum_{m\geq 0} c_{R,m}^{kh} = 2\pi(n_k I_k + n_h I_h) = 2\pi I_{kh}. \tag{33}$$

From these equations, we finally obtain

$$I_{kh} = -\sum_{m\geq 0} m b_{R,m}^{kh}. \tag{34}$$

Only a single action variable is determined in the two combined coordinates, because of the loss of independent freedom.

(ii) Island Motion. The Poincaré-Birkhoff fixed-point theorem[1] states that in the k–h coordinates, a baby (newly born) torus is generated encircling the elliptic fixed-points of the above primary resonance. Then a new frequency for this encircling motion (denoted by ω_{kh}^I) evolves, in addition to the original resonance frequency ω_{kh}^R of Eq. 26. Thus we have

$$\begin{aligned} B_{kh}(t) = a_R^{kh}t + \sum_{m\geq 0}\Big[b_{R,m}^{kh}\sin(m\omega_{kh}^R t) + c_{R,m}^{kh}\cos(m\omega_{kh}^R t)\Big] \\ + \sum_m \sin(m\omega_{kh}^R t)G_{R,m}^{kh}(t) \\ + a_I^{kh}t + \sum_{m\geq 0}\Big[b_{I,m}^{kh}\sin(m\omega_{kh}^I t) + c_{I,m}^{kh}\cos(m\omega_{kh}^I t)\Big] \\ + \sum_m \sin(m\omega_{kh}^I t)G_{I,m}^{kh}(t), \end{aligned} \tag{35}$$

where R and I stand for the resonance and island motions, respectively. This form is basically the same as the non-resonant case considered in Sect. II, and thus the action integrals for the two motions can be calculated separately as before.

If the further resonance (secondary and so on) takes place, where the commensurable relation between ω_{kh}^R and ω_{kh}^I happen to arise, we can go back to Eq. 25. The similar procedure is applied to the finer island motions.

III. Accurate Frequencies and Amplitudes from FFT Spectra

A. Procedure. In order to calculate the action variables in the above framework, the accurate frequencies and amplitudes are required beforehand. Not only

in our theory, determining accurate frequencies and amplitudes in a line spectrum can find many applications in any field of science and technology. The Fast Fourier Transformation (FFT) method is well-known as an ultra-fast technique and widely used. Practically, however, it is not easy to extract accurate frequencies and amplitudes from an FFT spectrum, because the grid (discretized) points representing frequencies are automatically given irrespective of the true frequencies desired to be computed. Further, in practical calculations only data sets of finite sampling length can be prepared. This truncation effect generates tails extending from all the FFT peaks, which is known as the Gibbs phenomenon. One of the general ways to suppress the tails is to use the window functions. A very clear report on the recent progress in the window techniques has been given by Martens and Ezra.[5] Generally speaking, however, the window techniques are quite tedious. Here we show a very simple alternative to pick up the accurate spectral data from raw (not biased by the windows) FFT spectrum. Since its full presentation has been given elsewhere,[8] only the outline of the idea is sketched here.

Let us consider a function of a form

$$\phi(t) = \sum_{m=1} [C_m \cos(mft) + S_m \sin(mft)]. \tag{36}$$

Our task is to find C_m, S_m, and f from the FFT spectrum. The extension to a system with many fundamental frequencies is straightforward. The cosine-FFT is usually defined in the following form

$$F_c(k) = \frac{2}{N} \sum_{j=0}^{N-1} \cos\left(\frac{2\pi kj}{N}\right) \sum_{m=1} [C_m \cos(mfj\Delta t) + S_m \sin(mfj\Delta t)], \tag{37}$$

where $\Delta t = T/N$, with T and N are the length and number of sampling points of the time series, respectively. The sine transformation $F_s(k)$ is defined in a similar way. Assuming that Δt is "sufficiently" small, the sum of Eq. 37 is *approximated* by the true Fourier integral such that

$$F_c(k) \cong \frac{2}{T} \int_0^T dt \cos\left(\frac{2\pi kt}{T}\right) \sum_{m=1} [C_m \cos(mft) + S_m \sin(mft)]. \tag{38}$$

Here, we have inverted the standard idea that FFT is an approximation to the true Fourier transformation. The integral of Eq. 38 is evaluated exactly as

$$F_c(k) \cong \sum_{m=1} \left[\frac{C_m}{T} \frac{\sin(mfT)}{mf - \frac{2\pi k}{T}} + \frac{C_m}{T} \frac{\sin(mfT)}{mf + \frac{2\pi k}{T}} - \frac{S_m}{T} \frac{\cos(mfT) - 1}{mf - \frac{2\pi k}{T}} - \frac{S_m}{T} \frac{\cos(mfT) - 1}{mf + \frac{2\pi k}{T}} \right]. \tag{39}$$

Suppose that the true frequency f happens to be located in the range

$$\frac{2\pi}{T} K < f < \frac{2\pi}{T}(K+1) \tag{40}$$

for a positive integer K. Such K can be identified easily by inspecting the FFT spectrum. Under this condition, $F_c(k)$ of Eq. 39 at $k=K$ and $k=K+1$ are far dominated by

$$F_c(K) \cong \frac{1}{T} \frac{C_1 \sin(fT) - S_1[\cos(fT) - 1]}{f - \frac{2\pi K}{T}} \tag{41a}$$

and

$$F_c(K+1) \cong \frac{1}{T} \frac{C_1 \sin(fT) - S_1[\cos(fT) - 1]}{f - \frac{2\pi(K+1)}{T}}. \tag{41b}$$

Then the ratio of Eq. 41a to Eq. 41b cancels the unknown quantities S_1 and C_1 as

$$X_c = \frac{F_c(K+1)}{F_c(K)} = \frac{f - \frac{2\pi K}{T}}{f - \frac{2\pi(K+1)}{T}}, \tag{42}$$

through which f can be guessed as

$$f \approx \frac{2\pi K}{T} - \frac{2\pi}{T} \frac{X_c}{1 - X_c}. \tag{43}$$

This is the first approximation to f.

Next the amplitudes S_m and C_m $(m=1,2,\cdots)$ are guessed with the least-square procedure minimizing

$$\sum_i \left[\phi(t_i) - \sum_{m=1} \{C_m \cos(mft_i) + S_m \sin(mft_i)\} \right]^2, \tag{44}$$

where t_i are sampling points, which should be selected so as to make the resultant linear equations non-singular. Thus the amplitudes are evaluated as the first approximation.

For the higher approximation to f, we return to Eq. 42. It should be remembered that both $F_c(K)$ and $F_c(K+1)$ are contaminated by the tails extended from the other peaks such as the harmonic frequencies and those associated with the other fundamental frequencies, if any. Now that the first approximations to the amplitudes are obtained, we can subtrast these tail components in such a way that

$$F_c'(K) = F(K) - \frac{2}{N} \sum_{m=2} \sum_{j=0}^{N-1} \cos\left(\frac{2\pi Kj}{N}\right) [C_m \cos(mfj\Delta t) + S_m \sin(mfj\Delta t)], \tag{45}$$

which gives the closer spectrum to the true one contributed only from the frequency f. The ratio in Eq. 42 is calculated again with these subtracted values $[F_c'(K)$ and $F_c(K+1)]$, and thereby the second guess of the frequency f is obtained. The improved frequencies are then brought back into Eq. 44 for the better amplitudes. The entire procedure should be repeated until a convergence is attained. Generally speaking, this convergence is very fast, which means that the first approximation of Eq. 43 already provides good values.

B. Numerical Example. Here we test our method by applying to the one-dimensional Morse oscillator problem, following Martens and Ezra,[5] the Hamiltonian of which is

$$H = \frac{p^2}{2} + (1 - e^{-q})^2. \tag{46}$$

This provides a stringent test, since the anharmonicity of the Morse potential is significant at the energy just below the dissociation limit. The analytical expressions of frequency and action variable are available[11] as the functions of energy E as

$$\omega(E) = [2(1-E)]^{1/2} \text{ and } I(E) = 2^{1/2}[1-(1-E)^{1/2}]. \tag{47}$$

We have picked up five energy points as the samples. (See Table 1) These energies correspond to the quantum numbers 1, 3, 5, 7, and 9, respectively, with the quantum number 10 being the highest of the system ($\hbar$=0.123 and the dissociation energy is 1.0). We have accumulated 5000 points to calculate $B'(t)$ by picking up one time regularly out of every 22 points to integrate the canonical equations of motion. The total time-length of this sampling is T=12500.513. Further, the sampling points for carrying out FFT with the size N=16384 (2^{14}) (Δt=0.762971) are generated with the spline interpolation. The resolution of frequency guaranteed by the present FFT is at most ($\Delta\omega$=) 0.0005. The frequencies and amplitudes have been determined by the method of Sect. IIB. Some 20 harmonics have been observed as visibly significant values in the power spectrum of $B'(t)$. In the present calculation, the harmonics up to the 90th have been taken into account just for the safety in Eq. 37. The number of the sampling points t_i for the least-square procedure in Eq. 44 is 190, which is also sufficiently large. The convergence of the iterated procedure to remove the tail effect is generally fast. In our all examples, the convergence has been attained within 3 iterations.

First, we examine the constant term of the Fourier spectrum of $B'(t)$, since it gives the action variable directly in one-dimensional cases. In Table 1 (column (a)) are listed the raw amplitudes at ω=0 obtained by the Fast-Fourier-cosine-transform. As stated in Sect. III A, the raw FFT spectra are contaminated by the tails extended from the other peaks, and accordingly not accurate. The refined values (column (b)) by removing the tail effect in the iterated procedure are shown also in Table 1. In order to check the identity of Eq. 22, the parts of the summation are calculated, too (column (c)). The each term $\omega m b_m$ (k=1 in Eq. 21) is calculated with the improved amplitude of the Fourier-cosine-transform of $B'(t)$. Table 1 has proved the validity of Eq. 22 quite clearly.

Table 1. The Constant Term of the Fourier Decomposition of $B'(t)$ in Various Representation

Energy	Crude[a]	Refined[b]	Sum[c]
0.243902	0.226863	0.226882	−0.226882
0.516154	0.423463	0.423489	−0.423489
0.727889	0.499456	0.499064	−0.499064
0.879109	0.453452	0.453609	−0.453609
0.969812	0.287255	0.287118	−0.287118

a) The raw value of the fast cosine transform of $B'(t)$ at ω=0. b) The improved value of the same quantity with the iteration method described in Sect. III B. c) The value of $\omega\Sigma m b_m$ to examine the validity and accuracy of Eq. 22.

Table 2 lists the frequencies and action variables. Our frequencies are essentially exact within the 6 significant digits. The action variables based on the crude a-value, picked up from the column (a) of Table 1, are not very accurate. On the other hand, the action variables based on Eq. 24 are extremely accurate (column (d) of Table 2), although very minor discrepancies have been found in the energies E=0.879109 and 0.969812.

IV. Quasi-Action Variable

A. Definition. In a domain where a system is not completely integrable, the action variables do not exist and the decomposition as in Eq. 15 looses its sense. Accordingly, the concepts of the fundamental frequency and its harmonics in Eq. 17 do not make sense either. On the other hand, the construction of $B'(t)$ such as Eq. 14 does not depend on the integrability. Therefore we can still find physical and/or mathematical meaning in the continuous Fourier transform of $B(t)$ and $B'(t)$. Even in chaos, it is convenient to expand $B'(t)$ in the form of FFT as

$$B'(t_j) = \sum_{h=0}^{[N/2]} \omega_h [b_h \cos(\omega_h t_j) - c_h \sin(\omega_h t_j)] \tag{48}$$

with the amplitudes being

$$\omega_h b_h = \frac{2}{N} \sum_{j=0}^{N-1} \cos(\omega_h t_j) B'(t_j) \tag{49a}$$

and

$$\omega_h c_h = -\frac{2}{N} \sum_{j=0}^{N-1} \sin(\omega_h t_j) B'(t_j), \tag{49b}$$

where

Table 2. The Frequencies and Action Variables for the Morse Oscillator

Energy	ω_{exact}[a]	ω_B[b]	I_{exact}[c]	I_B[d]	I_B[e]
0.243902	1.229714	1.229714	0.184500	0.184500	0.184484
0.516154	0.983713	0.983713	0.430500	0.430500	0.430475
0.727889	0.737714	0.737714	0.676500	0.676500	0.677032
0.879109	0.491713	0.491713	0.922500	0.922507	0.922188
0.969812	0.245715	0.245715	1.168498	1.168500	1.169059

a) The exact frequencies from Eq. 47. b) The frequencies through the FFT with the size of 2^{14}. The resolution of the frequency by the present FFT is 0.000503. c) The exact action variables from Eq. 47. d) The action variables by the expression Eq. 24. e) Approximate action variables evaluated with Eq. 23, where the a-values are obtained in the column (a) in Table 1.

$$\omega_h = \frac{2\pi h}{T} \quad \text{and} \quad t_j = \frac{T}{N} j = j\Delta t \tag{50}$$

and, as usual, N and T are the number and length, respectively, of the time series of the sampling points. It should be strongly noted that the coefficients b_h and c_h are both dependent of T in chaos, since no constant of motion other than the energy exists.

In Eq. 48, $B'(t)$ can be regarded as a linear combination of infinitely many harmonic contributions. For each harmonic oscillator, its action I_h, corresponding to the frequency ω_h, is written as [compare with Eq. 24]

$$I_h = \frac{1}{\omega_h}\left[(\omega_h b_h)^2 + (\omega_h c_h)^2\right]^{1/2}. \tag{51}$$

This expression has been written down lest it should depend on a particular choice of additive constants in the phases which can be considered in the following form

$$B'(t_j) = \sum_{h=0}^{[N/2]} \omega_h [b_h \cos(\omega_h t_j + \alpha_h) - c_h \sin(\omega_h t_j + \alpha_h)]. \tag{52}$$

It is thus only the power spectrum that has the invariant meaning with respect to these constant phases. Thus we define the quasi-action variable as a function of frequency as

$$\tilde{I}(\omega) = \frac{1}{\omega}\left\{\boldsymbol{P}[B'](\omega)\right\}^{1/2} = \frac{T}{2\pi}\left\{\boldsymbol{P}[B'](\omega)\right\}^{1/2}, \tag{53}$$

where $\boldsymbol{P}$ denotes the power spectrum of $B'(t)$, that is

$$\boldsymbol{P}[B'](\omega_h) = (\omega_h b_h)^2 + (\omega_h c_h)^2. \tag{54}$$

In an integrable case, on the other hand, $\tilde{I}(\omega)$ gives a set of discrete peaks with none-zero height

$$\tilde{I}(m\omega_k) \qquad k = 1, 2, \cdots, N; \quad m = 1, 2, \cdots. \tag{55}$$

at the fundamental, harmonic, and combination frequencies. When the component due to the fundamental frequency (m=1) is dominant, $\tilde{I}(\omega_k)$ is actually a very good approximation to the action variable. The quasi action is constant in the integrable cases.

The quasi-action gives discrete spectra in completely and nearly integrable systems. As chaos onsets, it becomes "continuous". By continuity, we mean a continuous spectrum observed within the scheme of FFT, which is not a perfectly continuous transformation. Incidentally, the generation of continuous spectrum in chaos has been numerically shown by Marcus and his colleague.[10,11] Further, in the continuous spectrum of the quasi-action variable, $1/f$-like-spectra can arise in view of the functional form of Eq. 53. We will see this aspect in the next section.

V. Example—Phase-Space Large Amplitude Motion

Some examples of the quasi-action variable are presented in what follows. The Hamiltonian adopted here is that of Hénon–Heiles,[12]

$$\boldsymbol{H} = \frac{p_x^2}{2m_x} + \frac{p_y^2}{2m_y} + \frac{1}{2}\left(x^2 + y^2 + 2x^2 y - \frac{2}{3}y^3\right), \tag{56}$$

where the masses are taken to be m_x=1.0 and m_y= 1.0087 throughout. The symmetry is broken by this slightly different choice of the mass balance. This Hamiltonian is well known to expose chaotic nature despite its simple form and has been extensively studied.[1] In the present paper, the trajectories with the total energy E=0.09 are mainly reported, because the onset of chaos can be clearly shown at this particular energy. The initial conditions of the trajectories are given in such a way that $x=y=0$, $p_x \geq 0$, $p_y \geq 0$, and the fraction of the energy assigned to the x-coordinate, denoted by f_x, is given parametrically.

Phase-Space Large Amplitude Motion. First, we observe in Fig. 4, that there is no potential barrier along the angular direction of the Hénon–Heiles potential function, which has C_3-symmetry. Nonetheless, we have dynamical barriers in the phase space, as can be clearly shown in the Poincaré surface of section[1] (Fig. 5). The equi-energy plane in phase space are divided into several cells. Each cell has a different mode of

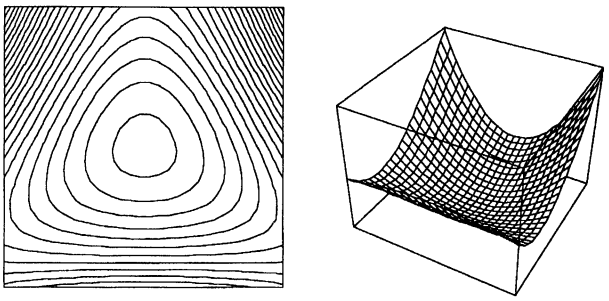

Fig. 4. Hénon–Heiles potential function. The contour plot and 3D perspective view.

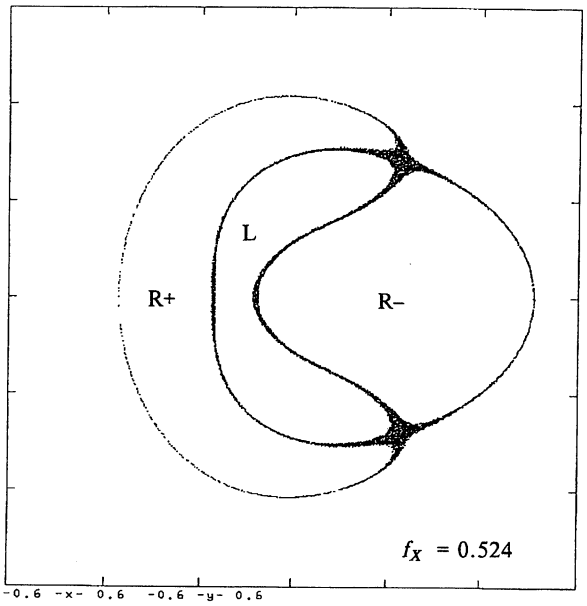

Fig. 5. The Poincaré section generated by a trajectory of E=0.09 and f_x=0.524.

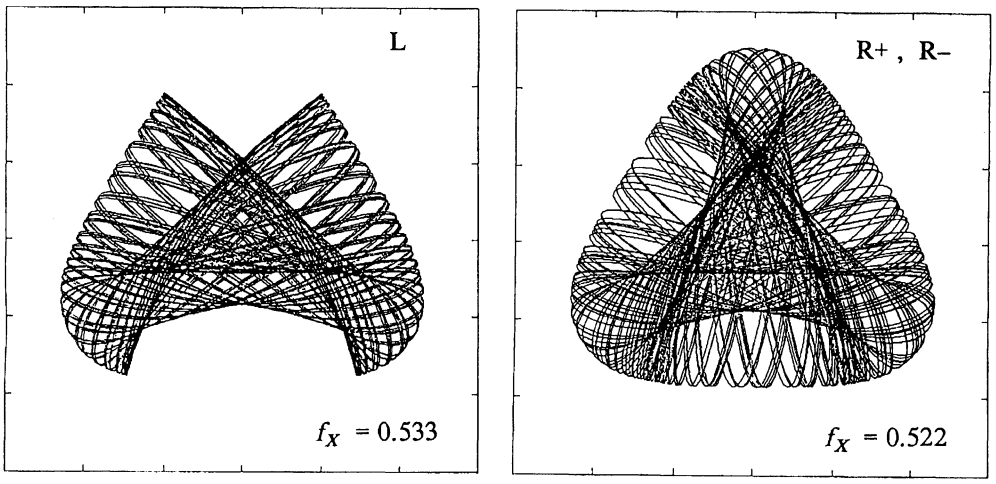

Fig. 6. The configuration-space view of the two different trajectories; libration (f_x=0.533) and rotation (f_x=0.522).

vibration that is recognized in the configuration space (Fig. 6). For example, the cell denoted by L is responsible for the libration mode as shown in Fig. 6, where a trajectory with f_x=0.533 is selected. On the other hand, we have two other cells corresponding to the rotational modes, one is left rotation and the other is right one. These two cannot be distinguished from each other in the static picture as in Fig. 6, where a trajectory with f_x=0.522 is shown. It is clear that the dynamical barrier separates the area as though there were a potential barrier in-between. However, since we have no apparent potential barrier to surmount, the situation is definitely different from the ordinary large-amplitude motion such as the umbrella motion of an ammonia molecule. It is surprising to see that a simple system with only two degrees of freedom can have such a variety of independent vibrational modes in the same energy range.

Our question is how the transition from one mode to another can take place. In our example of Fig. 6, what can happen if the initial-condition parameter f_x is change gradually from 0.533 to 0.522? The spectra of the quasi-action of these trajectories are shown in Figs. 7a and 7c, respectively, in which we show the part of frequency-range between 0.8 to 1.1 to compare only the main peaks. Apparently, these two modes can be clearly distinguished from the spectroscopic view point. Again, we ask how these two discrete spectra would compromise in becoming from one to the other. Here is the way they do. Figure 7b shows the spectrum of the quasi-action variable of a trajectory with f_x=0.524. This spectrum is continuous but the main peaks are almost superposition of two discrete spectra of Figs. 7a and 7c.

To see the time dependent behavior of the trajectory of f_x=0.524, we show $B'(t)$ in Fig. 8. Notice that there are basically two regularly oscillating patterns; one (called A) touched the bottom (the value zero) of the graph and the other (called B) not. This strongly suggests that the manifold on which the trajectory in the time domain B is clearly different from that of A. The validity of this statement is almost obvious from Eq. 14. $B'(t)$ can become very small, when the trajectory comes very close to the original point of t=0, or when the force vector happens to be parallel to the displacement vector $\vec{Z}(t)-\vec{Z}(0)$. The possibility of the latter case must be practically very small. Hence, in the region of B, the trajectory is supposed never to come close to the starting point of t=0 in phase space. Thus it is concluded that these two patterns indicate the existence of at least two distinctive manifolds. This is in fact confirmed in the Poincaré surface of section, Fig. 5. Incidentally, the similar analysis can be made in a larger system for which the Poincaré section is not available. Thus one can conclude that this trajectory runs with a definite mode (one among libration or rotations) for a certain period, but all of sudden, it turns into a different mode. These transitions continue forever, but it is virtually unpredictable exactly when they take place. So, macroscopically, this whole mode wandering among the individual modes can be regarded as a new kind of large amplitude motion in a wider region of phase space. We call this motion Phase-Space Large Amplitude Motion (PSLAM). More clear-cut behavior of the unpredictable character of PSLAM has been given elsewhere.[2)]

Correlation Decay. The above strange behavior is also confirmed in terms of the auto-correlation function defined by

$$C(t)=\frac{1}{T}\int_0^T d\tau[B'(t+\tau)-\langle B'\rangle][B'(\tau)-\langle B'\rangle]. \quad (57)$$

Since chaos is sometimes characterized as a process of loosing the memory[1,13)] the auto-correlation function has been widely used to study the correlation decay due to chaos. In our correlation function, we have chosen $B'(t)$, which is canonically invariant. It has turned out that this correlation function can detect the onset

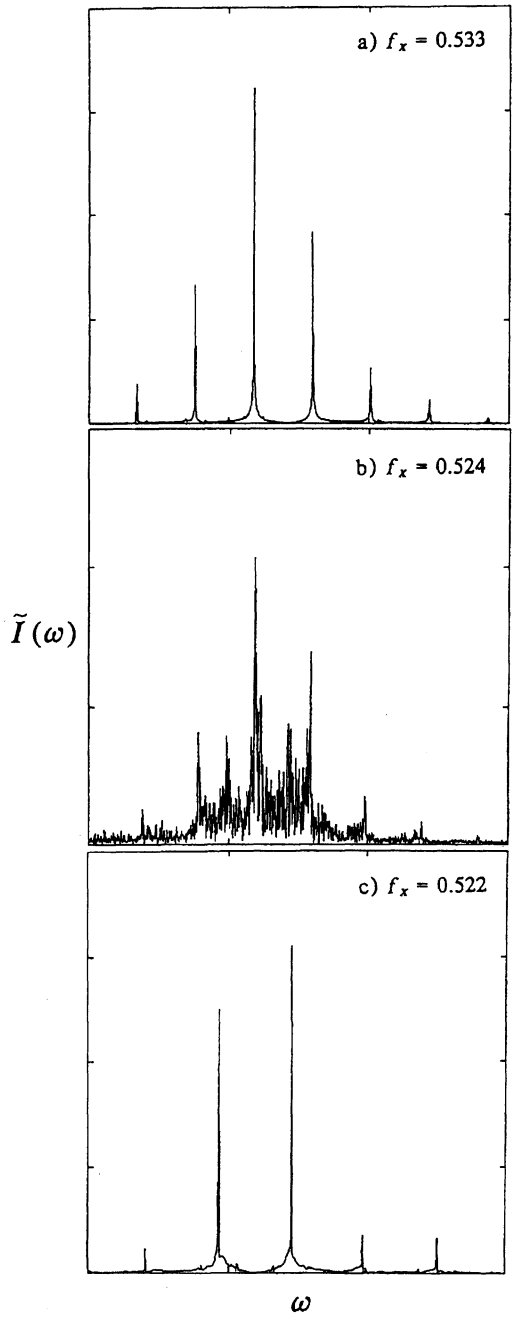

Fig. 7. The spectra of the quasi-action variables for the trajectories of (a) $f_x=0.533$, the sampling time $T=12000$, the height of the graph $H=0.4$, (b) $f_x=0.524$, $T=30000$, $H=0.15$, and (c) $f_x=0.522$, $T=12000$, $H=0.4$.

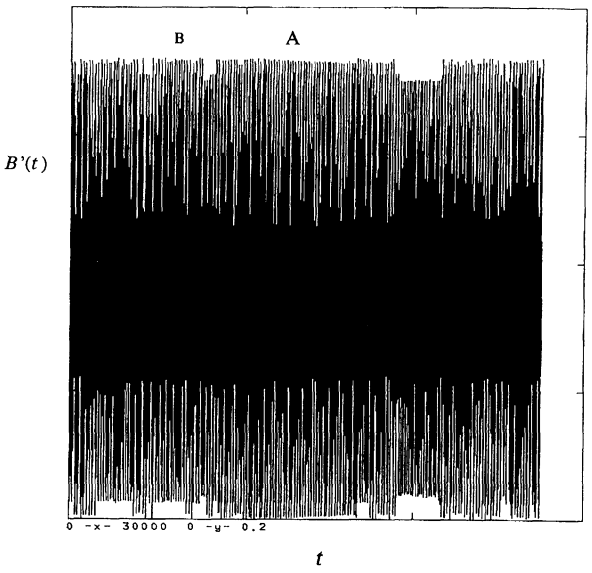

Fig. 8. $B'(t)$ to t for the trajectory of $E=0.09$ and $f_x=0.524$ [$0\leq t\leq 30000$]. The figure is basically composed of the two quasi-regular patterns. An intermittent-type chaos is observed; the transition takes place with unpredictable time and length.

of chaos with quite high sensitivity. Figure 9 shows the logarithmic plot of $|C(t)|$ versus t. In order to emphasize that this correlation decay is very slow and irregular (non-exponential), we provide an example of a typical exponential-decay due to a strong chaos in Fig. 10, which arises from a trajectory of the energy $E=0.16$ and $m_x=m_x=1.0$. The quasi-action in Fig. 11 also impresses how violent this chaos is. In Fig. 10, the finest oscillation represents the single beat of the local vibration with a period around $\omega\approx 0.8$—1.0 (see Fig. 11), and the small mountain shape in the envelope comes from the larger scale motions such as those we called libration and rotations in Fig. 6. The over-all exponential decay comes to its bottom line after 3 to 4 large scale motions. The exponential decay defined such that

$$C(t) \propto e^{-\alpha t} \tag{58}$$

can provide an alternative definition of entropy[1,13] associated with a single trajectory. The calculation is easy, and the resultant entropy is canonically invariant.

Here we make a detour to mention the time dependent property of the quasi-action variable in the strong chaos exemplified above. Since the quasi-action is not a conserved quantity in a chaotic domain, the quasi-action in Fig. 11 becomes lower and lower as the monitoring time-length (T) gets longer. In view of the complexity of the spectra, it is neither easy nor clear to measure the rate of the lowering behavior as a function of T. Nonetheless, we have observed the following two general properties: Basically the overall shape of the envelope does not change so much. So, the height at each frequency becomes lower uniformly with a similar rate. Furthermore, this lowering seems exponential with respect to T for the strong chaos at energy $E=0.16$. This would be consistent with the exponential decay of $|C(t)|$ as shown in Fig. 10.

As compared to the simple behavior of the strong chaos, the weak chaos as shown in Fig. 9 seems quite complicated. The envelope is not a simple exponential function and the decay time is very long. Nevertheless, the correlation decay can be clearly recognized.

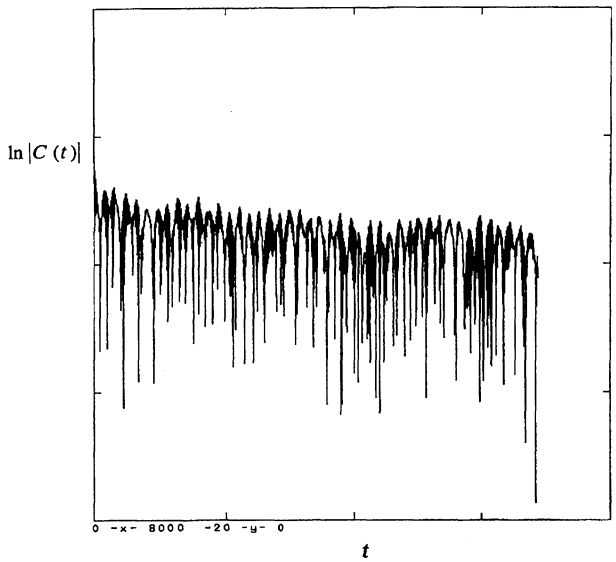

Fig. 9. $\ln|C(t)|$ to t for the trajectory of $E=0.09$ and $f_x=0.524$ $[0\leq t\leq 8000]$. Very slow and not a simple exponential decay is observed.

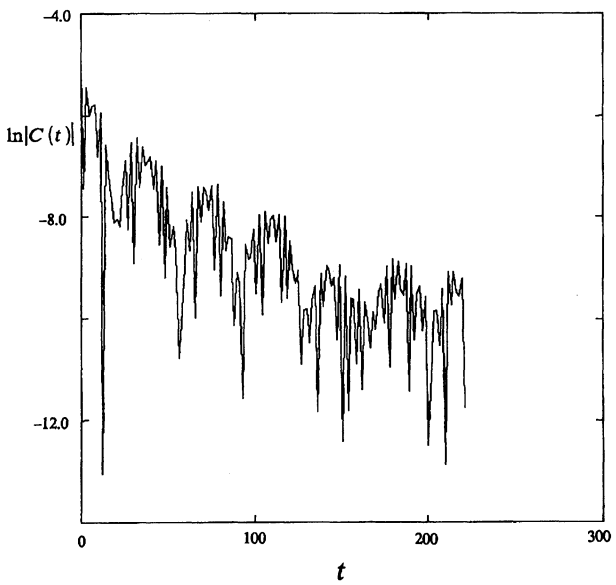

Fig. 10. The same as in Fig. 9 but for a trajectory $E=0.16$ $[0\leq t\leq 300]$. A typical exponential and quick decay of the correlation arises from the strong chaos.

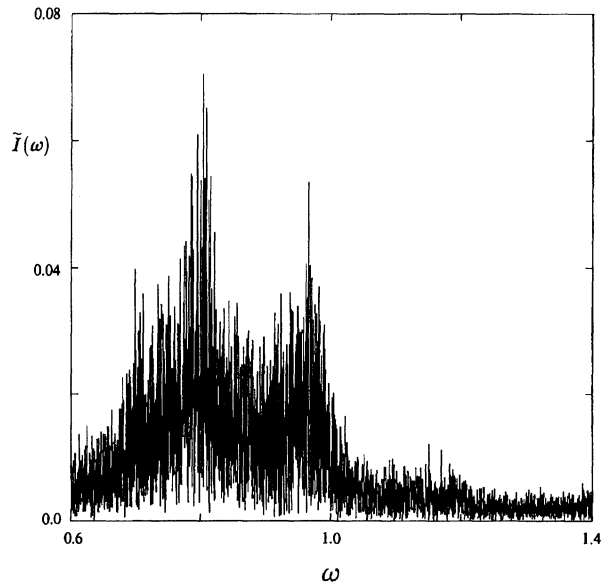

Fig. 11. The quasi-action vs. frequency for a strongly chaotic trajectory of $E=0.16$. The height of the graph $H=0.05$.

The first investigation of a time correlation function in chaos would be due to Mo,[14] whose work was examined in a great detail by Koszykowski, Noid, Tabor, and Marcus,[15,16] The function they chose was

$$a(t)=\sum_i\left[q_i(t)^2+p_i(t)^2\right] \tag{59}$$

and its variants, and the correlation functions based on the ensemble average were computed. We note that this quantity is not canonically invariant in contrast to $B'(t)$, although the physical meaning is rather appealing. It turned out[15] that the correlation function based on $a(t)$ decays irrespective of whether a system is chaotic or not. It is thus worthwhile emphasizing again that our correlation function clearly detect transition from non-decay to decay quite sharply.

1/f-Like-Spectrum or the Principle of Democracy. We now look at the small frequency region of the PSLAM of $E=0.09$ and $f_x=0.524$. Figure 12 shows a log–log plot of the quasi-action variable to t. A couple of noticeable peaks in the right part of the graph originate from the peaks at the frequencies around $\omega=1.0$ (see Fig. 7b). The spectrum keeps continuous down to the end point of the small frequency limit available. Furthermore, in the low frequency region, the quasi-action can be regarded as a $1/f$-spectrum. This seems not very

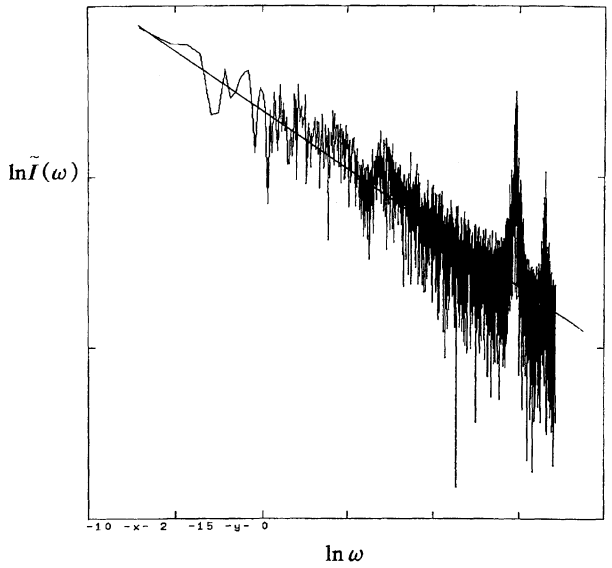

Fig. 12. $\ln\tilde{I}(\omega)$ to $\ln\omega$ for the trajectory of $E=0.09$ and $f_x=0.524$. In the small frequency range, $1/f$-type-spectrum appears. $[-10<\ln\omega<2,\ -15<\ln\tilde{I}(\omega)<0]$

surprising, if we look back at the definition of the quasi-action in Eq. 53, although the slope in Fig. 12 has small deviation from -1 to about -0.9. On the other hand, Eq. 53 also suggests that the power spectrum of $B'(t)$ itself should look like a white noise. It is this that is rather unexpected. The quasi-action variable provides a variant of the harmonic analysis, as suggested by the definition. The quasi-action at a given frequency ω can be interpreted as the product of the period ($T=2\pi/\omega$) of an imaginary harmonic-oscillator and the "probability" for the system (trajectory) to reside in that (see Eq. 53). This probability is represented by the power spectrum at that frequency as defined in Eq. 54. Thus, the fact that $\boldsymbol{P}[B'](\omega)$ looks almost a white noise means that almost all the imaginary harmonic-oscillators are shared with virtually equal probability. This also suggests that all the oscillators should have the similar energy, since the product in the left hand side of

$$\tilde{I}(\omega)\omega = \{\boldsymbol{P}[B'](\omega)\}^{1/2} \tag{60}$$

corresponds to the energy of the harmonic oscillator. (See Eq. 6 and its next line.) This situation reminds us of the so-called principle of equal a priori probability (or the principle of democracy). We also would like to stress that the quasi-action variable is an analog of the action variable which is one of the most fundamental observables in classical dynamics. Therefore, the $1/f$-like-spectrum arising from the fluctuation in classical chaos would imply the principle of equal a priori probability, through which the fundamental nature of statistical dynamics begins to enter.

Continuity Induced in Spectrum by "Non-Adiabatic Transitions". Finally, we investigate a little further the situation in which the discrete spectra change into the continuous ones. To this end, we look into the detailed structure of the quasi-action in the frequency range between 0.3 and 0.6 (Fig. 13), where the spectral lines, namely, the values of the quasi-action are far lower by a factor 100 than those of the main peaks of Figs. 7a and 7b. The fine structure of the spectra can be seen much more clearly in this range. First of all, Fig. 13a represents the trajectory of $f_x=0.533$. The higher peaks here are the combination bands due to the multiply-periodicity of the torus. The frequency difference between the neighboring major peaks represents the frequency of the libration mode. The small side-bands associated with the higher peaks arise from the fact that the trajectory is confined on a smaller torus that winds around its parent torus. The distinction of the macroscopically recognized mode, libration or rotations, are entirely due to the largest tori. The cross section of the smaller torus should be seen as a series of islands (the primary islands) on the Poincaré section.

An even more interesting example can be seen in Fig. 13b, in which the quasi-action of a trajectory of $f_x=0.5335$ is shown. This trajectory has an extremely long induction period before the chaotic motion manifests itself. During the precursory period, the mode appears as regular libration. Then the rotation comes in almost abruptly. Figure 13b represents the quasi-action for the precursory libration motion. We notice more violent island-motions. Here the secondary islands could be involved, which are in turn associated with the primary islands. The hierarchical sequence of the island structure is mathematically assured by the Birkhoff–Poincaré fixed-point theorem.[1,3] The development of the dense side-bands also means that motions having a very long time-scale are grown up. After the trajectory has entered into its macroscopically chaotic situation, which is still extremely weak in the sense that the transition from one mode to another is very rare, the side-band oscillations become even more violent as shown in Fig. 13c. The spread of the side-bands has been broadened so that they are tied up to each other. A little stronger chaos generated by a trajectory of $f_x=0.524$ evidences that all the isolated discrete lines are connected to each other to form a totally continuous spectrum covering the whole range of the frequency.

For the phase-space large amplitude motion that is composed of the independent macroscopic-motions, libration and rotations in the example here, the individual mode is not an adiabatic motion, even though each can have a long period. They are always modulated with the series of island motions, in other words, the macroscopic motions interact with the faster and smaller motions by exchanging the vibrational angular momentum.[2] The excess exchange of the vibrational angular momentum leads to the transition between the modes, i.e. from libration to rotation or vice versa.[17] This can be regarded as a classical analog of the so-called non-adiabatic transition commonly observed in

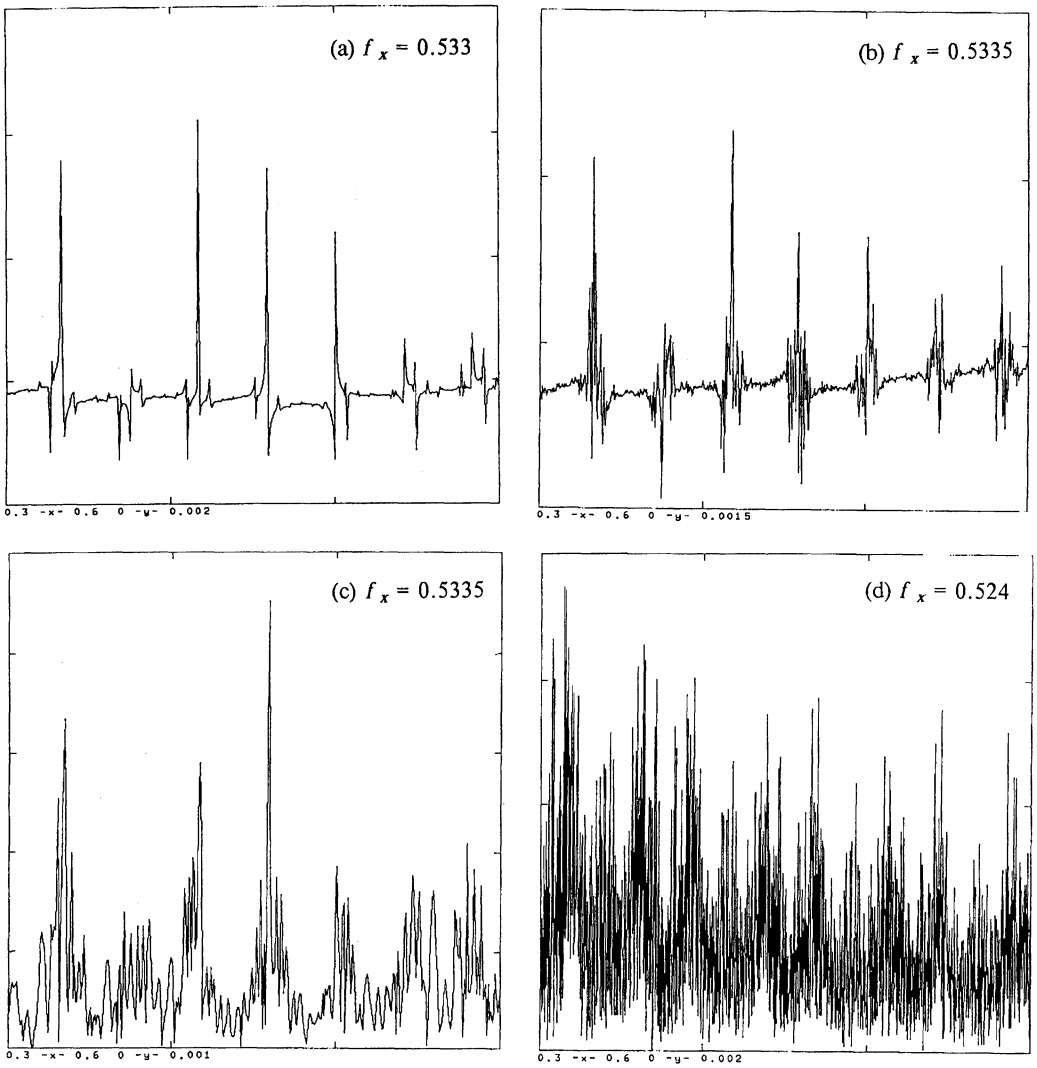

Fig. 13. The quasi-action variables in the frequency range [0.3, 0.6]. All the trajectories have $E=0.09$ with the following conditions. (a) $f_x=0.533$, the height of the graph $H=0.002$, (b) $f_x=0.5335$ in its very long induction period having the libration mode, $H=0.0015$, (c) $f_x=0.5335$ in the chaotic time-domain, $H=0.001$, (d) $f_x=0.524$, $H=0.002$.

quantum mechanics. In this sense, PSLAM is a macroscopic manifestation of the small non-adiabatic fluctuation. A further study is required for more detailed dynamics of the classically "non-adiabatic" transitions.

VI. Concluding Remarks

We have proposed the quasi-action variable as an analog to the action variable by considering a geometrical object that is canonically invariant in phase space. The quasi-action can be determined even in chaos. It gives a discrete spectrum in an integrable system and is transformed into a continuous spectrum as chaos takes place. Once chaos onsets, the quasi-action becomes smaller as the sampling time-interval gets longer, directly reflecting the fact that the quasi-action turns into a non-conservative quantity. The height of $\tilde{I}(\omega)$ as a function of the sampling time T, the decay of $C(t)$, the discreteness of $\tilde{I}(\omega)$ can all detect the clear-cut onset of chaos in a canonically invariant way. This indicates that these quantities are promising for the analysis and characterization of the mechanisms of chaos. A detailed analysis about the onset of chaos and the transport will be reported elsewhere.[17]

Some of the examples for the characteristics of the very weak chaos have been presented numerically, among which are (1) the non-exponential and very long-scale decay of the auto-correlation based on $B'(t)$, (2) $1/f$-like-spectrum of the quasi-action and its implication, and (3) the classical analog of the nonadiabatic transitions as a mechanism of the phase-space large amplitude motions.

An important practical aspect is that $B'(t)$, its spectra, and the quasi-action variable can all be computed very easily even for a large system of chemical interest, as far as the classical trajectory calculation can be carried out. Although we have shown the examples of a

very small system in the present paper, this definitely does not imply its practical limitation. On the contrary, we conceive that the PSLAM can be a prototype of the dynamics of structural transition or the so-called re-clustering dynamics of a large molecular system.[18] This study is currently under way.

Finally, we conclude this paper by noting again that the action variables can be actually extracted from the Fourier spectrum of $B'(t)$. In this conjunction, a method has been invented to calculate very accurate frequencies and amplitudes from an FFT spectrum without using the window technique. In the present paper, the calculation of the action variables is not of primary interest. However, it would be right to say that our theory provides one of the simplest methods so far proposed. Since the semiclassical quantization with the EBK conditions of a multi-dimensional system is still a difficult problem and practically important in the study of molecular vibration,[5,6,19,20] it is expected that this part of the present work could find useful applications in chemical dynamics.

This work was supported in part by the Grant in Aid from the Ministry of Education, Science and Culture.

References

1) For a comprehensive review on classical chaos, see: A. J. Lichtenberg and M. A. Lieberman, "Regular and Stochastic Motion," Springer, Berlin (1983).
2) K. Takatsuka, *Chem. Phys. Lett.*, **204**, 491 (1993).
3) a) V. I. Arnold, "Mathematical Methods of Classical Mechanics," Springer, Berlin (1978); b) R. Abraham and J. E. Marsden, "Foundation of Mechanics," 2nd ed, Addison-Wesley, Reading (1985); c) H. Goldstein, "Classical Mechanics," Addison-Wesley, Reading (1980).
4) See for example: I. C. Percival, *Adv. Chem. Phys.*, **36**, 1 (1976), and references therein.
5) C. C. Martens and G. S. Ezra, *J. Chem. Phys.*, **83**, 2990 (1985).
6) C. C. Martens and G. S. Ezra, *J. Chem. Phys.*, **86**, 279 (1986).
7) I. C. Percival, *J. Phys. A: Gen. Phys.*, **7**, 794 (1974).
8) K. Takatsuka, *J. Comput. Phys.*, **102**, 374 (1992).
9) See for example: O. Brigham, "The Fast Fourier Transform," Prentice Hall, New Jersey (1974).
10) M. L. Koszykowski, D. W. Noid, and R. A. Marcus, *J. Phys. Chem.*, **86**, 2113 (1982).
11) D. W. Noid, M. L. Koszykowski, and R. A. Marcus, *J. Chem. Phys.*, **67**, 404 (1977).
12) M. Hénon and C. Heiles, *Astron. J.*, **69**, 73 (1964).
13) R. Z. Sagdeev, D. A. Usikov, and G. M. Zaslavsky, "Nonlinear Physics," Harwood, London (1988).
14) K. C. Mo, *Physica*, **57**, 455 (1972).
15) M. L. Koszykowski, D. W. Noid, M. A. Tabor, and R. A. Marcus, *J. Chem. Phys.*, **74**, 2530 (1982).
16) M. A. Tabor, *Adv. Chem. Phys.*, **46**, 73 (1981).
17) K. Takatsuka, to be published.
18) For example, see: I. Ohmine and H. Tanaka, *J. Chem. Phys.*, **93**, 8138 (1990), and references cited therein.
19) R. Ramaswamy, *J. Chem. Phys.*, **82**, 747 (1985).
20) S. Sinha and R. Ramaswamy, *Mol. Phys.*, **67**, 335 (1989).